Inorganic Chemistry
Article

Inorg. Chem. **2010**, *49*, 3057–3063 **3057**
DOI: 10.1021/ic100276z

Synthesis, Structure, and Phosphatase-Like Activity of a New Trinuclear Gd Complex with the Unsymmetrical Ligand H_3L As a Model for Nucleases

Maryene A. Camargo,[†] Ademir Neves,[*,†] Bruno Szpoganicz,[†] Adailton J. Bortoluzzi,[†] Franciele L. Fischer,[‡] Hernán Terenzi,[‡] and Eduardo E. Castellano[§]

[†]*Laboratório de Bioinorgânica e Crystalografia (LABINC), Departamento de Química, Universidade Federal de Santa Catarina, 88040-900 Florianópolis, Santa Catarina, Brazil,* [‡]*Laboratório de Expressão Gênica, Departamento de Bioquímica, CCB, Universidade Federal de Santa Catarina, 88040-900 Florianópolis, Santa Catarina, Brazil, and* [§]*Instituto de Física, Universidade de São Paulo,13560-970 São Carlos, São Paulo, Brazil*

Received February 10, 2010

The new trinuclear gadolinium complex $[Gd_3L_2(NO_3)_2(H_2O)_4]NO_3 \cdot 8H_2O$ (**1**) with the unsymmetrical ligand 2-[*N*-bis-(2-pyridylmethyl)aminomethyl]-4-methyl-6-[*N*-bis(2-hydroxy-2-oxoethyl)aminomethyl] phenol (H_3L) was synthesized and characterized. The new ligand H_3L was obtained in good yield. Complex **1** crystallizes in an orthorhombic cell, space group *Pcab*. Kinetic studies show that complex **1** is highly active in the hydrolysis of the substrate 2,4-bis(dinitrophenyl)phosphate (K_m = 4.09 mM, $V_{max} = 2.68 \times 10^{-2}$ mM s^{-1}, and $k_{cat} = V_{max}/[\mathbf{1}] = 0.67\ s^{-1}$). Through a potentiometric study and determination of the kinetic behavior of **1** in acetonitrile/water solution, the species present in solution could be identified, and a trinuclear monohydroxo species appears to be the most prominent catalyst under mild conditions. Complex **1** displays high efficiency in DNA hydrolytic cleavage, and complete kinetic studies were carried out ($K_m = 4.57 \times 10^{-4}$ M, $k'_{cat} = 3.42\ h^{-1}$, and $k'_{cat}/K_m = 7.48 \times 10^3\ M^{-1}\ h^{-1}$). Studies with a radical scavenger (dimethyl sulfoxide, DMSO) showed that it did not inhibit the activity, indicating the hydrolytic action of **1** in the cleavage of DNA, and studies on the incubation of distamycin with plasmid DNA suggest that **1** is regio-specific, interacting with the minor groove of DNA.

Introduction

Phosphodiesters are well-known for both their importance as biomolecules (as components of DNA and RNA, for example) and their stability. Thus, considerable efforts are being made to develop catalytic systems (artificial nucleases) capable of cleaving efficiently phosphodiester bonds.[1−4] As with natural nucleases, a hydrolytic rather than oxidative cleavage mechanism is desirable for molecular biology and clinical applications. Thus, there is an open field for the development of lanthanide-based nucleases: even the Ce^{IV} ion, the lanthanide with the highest redox activity, acts as a hydrolytic catalyst.[5]

In nature, a large number of metalloenzymes able to catalyze phosphate ester hydrolysis are activated by two or more metal ions (at the active site of the enzyme). Jurek and co-workers have reported cooperativity between two La^{III} ions in a dinuclear complex which is more reactive toward phosphate diester hydrolysis than the similar mononuclear species.[6] Dinuclear complexes are able to produce nucleophile hydroxo groups at lower pH values, making these species prominent catalysts in hydrolysis reactions.

Several systems are used in the coordination with lanthanide ions, such as polyhydroxyl ligands,[7] crown ethers and azacrowns,[8,9] and polyaminocarboxylate derivatives,[10] and so forth. These systems avoid the precipitation of $Ln(OH)_3(s)$ and provide compounds with a positive overall charge favoring, consequently, the catalytic action toward the hydrolysis of phosphate esters. Branum and Que reported La^{III} and Ce^{IV} ions combined with the dinucleating ligand HPTA, which represent the first metal complexes capable of carrying out hydrolysis of double-stranded DNA.[11]

*To whom correspondence should be addressed. E-mail: ademir@qmc.ufsc.br.

(1) Liu, C.; Wang, M.; Zhang, T.; Sun, H. *Coord. Chem. Rev*. **2004**, *248*, 147–168.
(2) Mitić, N.; Smith, S. J.; Neves, A.; Guddat, L. W.; Gahan, L. R.; Schenk, G. *Chem. Rev*. **2006**, *106*, 3338–3363.
(3) Gahan, L. R.; Smith, S. J.; Neves, A.; Schenk, G. *Eur. J. Inorg. Chem*. **2009**, 2745–2758.
(4) Jarenmark, M.; Carlsson, H.; Nordlander, E. *C. R. Chim*. **2007**, *10*, 433–462.
(5) Shigekawa, H.; Ishida, M.; Miyake, K. *Appl. Phys. Lett*. **1999**, *74*, 460–463.
(6) Jurek, P. E.; Jurek, A. M.; Martell, A. E. *Inorg. Chem*. **2000**, *39*, 1016–1020.
(7) Gomez-tagle, P.; Yatsimirsky, A. K. *Inorg. Chem*. **2001**, *40*, 3786–3796.
(8) Peluffo, F.; Torres, J.; Kremer, C.; Dominguez, S.; Mederos, A.; Kremer, E. *Inorg. Chim. Acta* **2006**, *359*, 2107–2114.
(9) Belousoff, M. J.; Ung, P.; Forsyth, C. M.; Tor, Y.; Spiccia, L.; Graham, B. *J. Am. Chem. Soc*. **2009**, *131*, 1106–1114.
(10) Torres, J.; Brusoni, M.; Peluffo, F.; Kremer, C.; Dominguez, S.; Mederos, A.; Kremer, E. *Inorg. Chim. Acta* **2005**, *358*, 3320–3328.
(11) Branum, M. E.; Que, L., Jr. *J. Biol. Inorg. Chem*. **1999**, *4*, 593–600.

Published on Web 02/19/2010

In this paper, we present the synthesis of the new 2-[*N*-bis-(2-pyridylmethyl)aminomethyl]-4-methyl-6-[*N*-bis(2-hydroxy-2-oxoethyl)aminomethyl]phenol ligand (H_3L) and the synthesis and structure of its trinuclear $[Gd_3L_2(NO_3)_2(H_2O)_4]$-$NO_3 \cdot 8H_2O$ (**1**) complex, which displays high activity toward the hydrolysis of the activated substrate 2,4-bis(dinitrophenyl)phosphate (BDNPP). Complex **1** was found to be active toward the hydrolytic cleavage of plasmid DNA, interacting with regio-specificity, indicating its potential action as a chemical nuclease.

Experimental Section

Abbreviations. The following abbreviations are used in this paper: H_3L, 2-[*N*-bis-(2-pyridylmethyl)aminomethyl]-4-methyl-6-[*N*-bis(2-hydroxy-2-oxoethyl)aminomethyl]phenol; HPTA, 1,3-diamino-2-hydroxypropane-*N*,*N*,*N*′,*N*′-tetraacetate; BDNPP, 2,4-bis(dinitrophenyl)phosphate; DNPP, 2,4-dinitrophenyl phosphate; DNP, 2,4-dinitrophenolate; ESI-MS, electrospray ionization−mass spectrometry; BTP, 1,3-bis[tris(hydroxymethyl)methylamino]propane; bp, base pairs; DMSO, dimethyl sulfoxide.

Materials and Measurements. BDNPP and ligand **2** were synthesized by previously described methods.[12−14] All other chemicals and solvents were of analytical or spectroscopic grade purchased from commercial sources, and used without further purification. Infrared spectra were recorded on a Perkin-Elmer model 16PC spectrometer, in KBr pellets in the 4000−400 cm^{-1} range. ^1H NMR and ^{13}C NMR spectra were recorded on a Varian Mercury Plus 400 spectrometer (400 and 100 MHz, respectively) in $CDCl_3$ or D_2O and using tetramethylsilane (TMS, δ = 0.00 ppm) as the internal standard. Elemental analysis was performed on a Carlo Erba E-1110 instrument. The mass spectrometry (MS) experiments were carried out using a Q-TOF mass spectrometer (Micromass, Manchester, U.K.) and electrospray ionization in the positive mode (ESI(+)-MS). Typical MS conditions were as follows: source temperature of 100 °C, desolvation temperature of 100 °C, capillary voltage of 3 kV, and cone voltage of 50 V. The sample was injected using a syringe pump (Harvard Apparatus) at a flow rate of 5 μL/min. Mass spectra were acquired within the range of 50−2000 m/z.

Preparation of 2-[*N*-bis-(2-pyridylmethyl)aminomethyl]-4-methyl-6-[*N*-bis(2-methoxy-2-oxoethyl)aminomethyl]phenol (3). Ligand **2**[13,14] (0.01 mol; 4.21 g), dimethyl iminodiacetate (0.01 mol; 1.68 g), and triethylamine (0.02 mol; 2.90 mL) were dissolved in 100 mL of dichloromethane in a 125 mL flask. The reaction mixture was refluxed for 24 h and then stirred for 72 h at room temperature. The resultant solution was washed with a saturated solution of $NaHCO_3$ (6 × 30 mL), dried with Na_2SO_4, and evaporated under vacuum to yield product **3** as a viscous liquid. Yield: 91%. Selected IR data (KBr): ν (C−H_{Ar} and C−H_{Aliph}) 3052−2842; ν (C═C and C═N) 1590−1434; δ (O−H) 1372; ν (C−O_{phenol} and C−O_{ester}) 1296−1150; ν (C═O) 1743; δ (C−H_{Ar}) 764 in cm^{-1}. ^1H NMR δ_H (400 MHz; $CDCl_3$): 2.23 (3 H, s, CH_3); 3.60 (4 H, s, CH_2); 3.71 (6H, s, CH_3); 3.80 (2 H, s, CH_2); 3.90 (4 H, s, CH_2); 3.96 (2 H, s, CH_2); 6.95 (2H, d, CH_{Ar}); 7.14−7.17 (2H, m, CH_{Ar}); 7.43−7.45 (2H, m, CH_{Ar}); 7.63−7.64 (2H, m, CH_{Ar}); 8.54−8.56 (2H, m, CH_{Ar}) in ppm. ^{13}C NMR δ (100 MHz; $CDCl_3$): 20.69; 51.84; 53.36; 54.44; 55.83; 59.48; 122.42; 123.23; 123.49; 127.99; 130.69; 130.83; 136.97; 149.10; 153.86; 158.44; 171.97 in ppm.

Preparation of 2-[*N*-bis-(2-pyridylmethyl)aminomethyl]-4-methyl-6-[*N*-bis(2-hydroxy-2-oxoethyl)aminomethyl]phenol (H_3L). Ligand **3** (2.65 mmol; 1.30 g) was dissolved in 40 mL of methanol, and then KOH (18.52 mmol; 1.04 g) was added. This mixture was stirred for 4 days at room temperature. The resultant solution was dried under vacuum. The residual solid obtained was dissolved in 10 mL of deionized water solution and neutralized with HCl (4 mol L^{-1}) to pH 7. Subsequent chromatographic purification with basic DOWEX (1 × 2:200) eluted with acetic acid led to H_3L. Yield: 90%. Selected IR data (KBr): ν (O−H, C−H_{Ar} and C−H_{Aliph}) 3551−2924; ν (C═C and C═N) 1600−1430; ν (COO^-) 1631 and 1398; δ (C−H_{Ar}) 764 in cm^{-1}. ^1H NMR δ_H (400 MHz; D_2O): 1.85 (s, 3 H, CH_3−residue of CH_3COOH); 1.98 (s, 3 H, CH_3); 3.54 (s, 4 H, CH_2); 3.72 (s, 2H, CH_2); 4.01 (4H, s, CH_2); 4.09 (2H, s, CH_2); 6.82 (2H, d, CH_{Ar}); 7.39 (4H, d, CH_{Ar}); 7.87 (2H, t, CH_{Ar}); 8.41 (2H, d, CH_{Ar}) in ppm. ^{13}C NMR δ (100 MHz; D_2O): 19.27; 21.05; 55.63; 56.24; 56.86; 57.74; 116.94; 122.64; 124.96; 125.97; 130.56; 133.19; 133.94; 142.48; 144.90; 152.75; 153.24; 170.39; 177.71 (residue of CH_3COOH) in ppm.

Synthesis of $[Gd_3L_2(NO_3)_2(H_2O)_4]NO_3 \cdot 8H_2O$ (1). Complex **1** was prepared by adding $Gd(NO_3)_3 \cdot 6H_2O$ to a methanolic solution containing the ligand H_3L and NaOH (3:2:6 stoichiometry), under magnetic stirring at 40 °C for 40 min. After total solvent evaporation, the solid obtained was recrystallized in a methanol/ethanol/acetone (1:1:1) solution mixture, yielding colorless monocrystals suitable for X-ray analysis. Yield: 20%. Found: C, 32.21; H, 4.18; N, 8.50. Calcd for $[Gd_3(C_{25}H_{25}N_4O_5)_2(NO_3)_2(H_2O)_4]NO_3 \cdot 8H_2O$: C, 33.42; H, 4.15; N, 8.57. Selected IR data (KBr): ν (O−H, C−H_{Ar} and C−H_{Aliph}) 3550−2922; ν (C═C and C═N) 1602−1450; ν (C−O_{phenol}) 1256 and 1228; ν (COO^-) 1654 and 1450; ν (NO_3^-) 1482, 1386, and 1295; δ (C−H_{Ar}) 786 in cm^{-1}. ESI-MS: $[Gd_3L(NO_3)_3(CH_3CN)_6(H_2O)_6]^{3+}$ m/z 492; $[Gd_3L(NO_3)_3$-$(CH_3CN)_5(H_2O)_6]^{3+}$ m/z 478; $[Gd_3L(NO_3)_3(CH_3CN)_4$-$(H_2O)_6]^{3+}$ m/z 464 (only fragment ions were observed, probably because of the gas-phase conditions).

Single-Crystal X-ray Structure Determination. A fragment with dimensions of 0.26 × 0.44 × 0.47 mm^3 was selected from a crystalline sample of complex **1** for crystallographic analysis. X-ray diffraction data were measured on a Kappa-CCD diffractometer with graphite-monochromated Mo Kα (λ = 0.71073 Å) radiation, at room temperature. Diffraction data were collected (φ and ω scans with *K*-offsets) with COLLECT.[15] Integration and scaling of the reflections were performed with HKL DENZO-SCALEPACK suite of programs. The unit cell parameters were obtained by least-squares refinement based on the angular settings for all collected reflections using HKL SCALEPACK.[16] Gaussian absorption correction was applied to the collected reflections with PLATON,[17] with maximum and minimum transmission factors of 0.496 and 0.278, respectively. The structure was solved by direct methods and refined by full-matrix least-squares on F^2.[18] All non-hydrogen atoms were refined with anisotropic displacement parameters. Hydrogen atoms bond to C atoms were placed at their idealized positions using standard geometric criteria. H atoms of the coordinated and uncoordinated water molecules could not be located from the Fourier difference map. Further crystallographic information is presented in Table 1.

Full tables containing the crystallographic data (except structure factors) were deposited at Cambridge Structural Database (CCDC 752704) and these data are available free of charge at www.ccdc.cam.ac.uk.

Potentiometric Titrations. The potentiometric studies were carried out with a Corning-350 research pH meter fitted with blue-glass and Ag/AgCl reference electrodes calibrated to read

(12) Bunton, C. A.; Farber, S. J. *J. Org. Chem.* **1969**, *34*, 767–772.
(13) Karsten, P.; Neves, A.; Bortoluzzi, A. J.; Lanznaster, M.; Drago, V. *Inorg. Chem.* **2002**, *41*, 4624–4626.
(14) Lambert, E; Chabut, B.; Chardon-Noblat, S; Deronzier, A; Chottard, G.; Bousseksou, A; Tuchagues, J.-P.; Laugier, J.; Bardet, M.; Latour, J.-M. *J. Am. Chem. Soc.* **1997**, *119*, 9424–9437.
(15) *COLLECT*; Enraf-Nonius BV: Delft, The Netherlands, 2000.
(16) Otwinowski, Z.; , Minor, W. In *Methods Enzymol.*; Carter, C. W., Jr., Sweet, R.M., Eds.; Academic Press: New York, 1997; Vol. *2*, p 307.
(17) Spek, A. L. *Acta Crystallogr.* **2009**, *D65*, 148–155.
(18) Sheldrick, G. M. *Acta Crystallogr.* **2008**, *A64*, 112–122.

Table 1. Crystallographic Data and Structure Refinement for Complex **1**

empirical formula	$C_{50}H_{74}Gd_3N_{11}O_{31}$	
formula weight	1796.95	
temperature	296(2) K	
wavelength	0.71073 Å	
crystal system	orthorhombic	
space group	*Pbca*	
unit cell dimensions	a = 27.0964(7) Å	α = 90°.
	b = 17.7944(5) Å	β = 90°.
	c = 27.4867(5) Å	γ = 90°.
volume	13253.1(6) Å^3	
Z	8	
density (calculated)	1.801 Mg/m^3	
absorption coefficient	3.063 mm^{-1}	
F(000)	7128	
crystal size	0.47 × 0.44 × 0.26 mm^3	
θ range for data collection	2.61 to 26.00°.	
index ranges	$-17 \le h \le 33$	
	$-21 \le k \le 10$	
	$-33 \le l \le 27$	
reflections collected	38608	
independent reflections	12995 [R(int) = 0.0592]	
refinement method	full-matrix least-squares on F^2	
data/restraints/parameters	12995/0/856	
goodness-of-fit on F^2	1.091	
final R indices [$I > 2\sigma(I)$]	R1 = 0.0445, wR2 = 0.1238	
R indices (all data)	R1 = 0.0615, wR2 = 0.1353	
largest diff. peak and hole	1.897 and −2.432 e Å^{-3}	

−log [H+] directly. The electrode was calibrated using the data obtained from the potentiometric titration of a known volume of a standard 0.10 mol L^{-1} HCl solution with a standard 0.10 mol L^{-1} KOH solution. The ionic strength of the HCl solution was maintained at 0.10 mol L^{-1} by addition of KCl. Measurements were carried out in a thermostatted cell containing a solution of the complex (0.05 mol/50 mL) with ionic strength adjusted to 0.10 mol L^{-1} by addition of KCl, at 25.00 ± 0.05 °C. The experiments were performed under argon to eliminate the presence of atmospheric CO_2. All of the experimental solutions were prepared in acetonitrile/water (1:1, v/v) owing to the low solubility of the complex in water. The pK_w of the acetonitrile/water containing 0.10 mol L^{-1} of KCl used was 15.40.[19] Computations were carried out with the BEST7 program, and species diagrams were obtained with SPE and SPEPLOT programs.[20]

Reactivity. Kinetic experiments for the hydrolysis of the model substrate bis(2,4-dinitrophenyl)phosphate (BDNPP) were followed spectrophotometrically for the absorbance increase at 400 nm (ε = 12100 L mol^{-1} cm^{-1}) because of the formation of 2,4-dinitrophenolate (DNP) over time, under conditions of excess substrate at 25 °C. In these experiments, all of the solution mixtures were in an acetonitrile/water (3:1 v/v) medium, owing to the low solubility of the complex in water under the concentration conditions used. The systems showed high catalytic activity, and their study was only possible through the stopped-flow technique. The stopped-flow apparatus (model SX-18MV) and the associated computer system were manufactured by Applied Photophysics. The data were analyzed with the SX-18MV operating software. A total of 150 μL per sample was transferred to a 1 cm thermostatically controlled cell compartment. The experiments were carried out in triplicate. Reactions were monitored during the first seconds, and the data treated using the initial rate method. Initial rates were obtained directly from the plot of the DNP concentration versus time under the same experimental conditions. Studies on the effects of pH on the hydrolysis reaction were performed in the pH range of 3.5−10.0 (MES pH 3.5−6.5; HEPES pH 7.0−8.0; CHES pH 9.0−10.0; I = 0.1 mol L^{-1} with $LiClO_4$), under a 50-fold excess of substrate, at 25 °C. Experiments to determine the dependence of the reaction rate on the substrate concentration (5×10^{-4} to 5×10^{-3} mol L^{-1}) were carried out at 25 °C, pH 6.0, with complex **1** (4×10^{-5} mol L^{-1}). Because of the lower solubility of the reagents, these were the best concentration conditions for obtaining the kinetic parameters. To establish the number of molecules of substrate which are hydrolyzed per molecule of complex, the reaction was monitored at 445 nm, under a 50-fold substrate excess at pH 6.0 and 25 °C.

DNA Cleavage. The plasmid pBSK II (2961 bp), used for the DNA cleavage assays, was purchased from Stratagene, transformed into DH5α *Escherichia coli* competent cells and amplified as previously described.[21] The plasmid DNA was extracted from *E. coli* and purified using the Qiagen Plasmid Maxi Kit protocol.[22] The DNA cleavage activity of **1** was determined by following the conversion of supercoiled plasmid DNA (FI) to open circular DNA (FII) and/or linear DNA (FIII) using agarose gel electrophoresis to separate the cleavage products. In general, 520 ng of pBSK II (40 μM in pb) in 25 mM PIPES buffer (pH 6.5, 7.0 and 7.5) or HEPES buffer pH 8.0 were treated with different concentrations of **1** (10−125 μM) in CH_3CN (25% in reaction volume) for 7 h at 50 °C (complex **1** displayed low activity at 25 °C and, consequently, the kinetic parameters could not be obtained at this temperature). Thereafter, each reaction was quenched adding 5 μL of a loading buffer solution (0.01% bromophenol blue, 50% glycerol, and 250 mM EDTA pH 8.0) and then subjected to electrophoresis on a 0.8% agarose gel containing 0.3 μg.mL^{-1} of ethidium bromide in 0.5 × TBE buffer (44.5 mM Tris, 44.5 mM boric acid, and 1 mM EDTA) at 90 V for approximately 1.5 h. The resulting gels were visualized and digitized with a photo documentation system (UVP Inc., Upland, CA, U.S.A.). The ratio of DNA in each band was quantified using LabWorks software version 4.0 (UVP). The ratio of supercoiled DNA was increased by a factor of 1.47, since the ability of ethidium bromide to intercalate into this topoisomeric form is lower relative to circular and linear forms.[23] To study the involvement of hydroxyl radicals in the mechanism of the DNA cleavage performed by **1**, 10% DMSO was added to the reaction mixtures prior to addition of the complex. To determine the DNA major or minor groove selectivity of **1**, assays were performed using the minor groove binder distamycin (50 μM), or the major groove binder methyl green (50 μM). The plasmid DNA was pretreated with the groove binder for 30 min at room temperature, and then the complex was added and the reaction was incubated as described above. The DNA cleavage rates (k_{obs}) promoted by **1** were determined treating the plasmid DNA at different complex concentrations (10−250 μM) for different time intervals (0−6 h). The k_{obs} were calculated for each complex concentration assuming a pseudo-first-order kinetics and then analyzed following the pseudo-Michaelis−Menten formalism.[24] The reaction conditions were as described above.

Results and Discussion

Syntheses. The synthetic route used for the preparation of the unsymmetrical ligand H_3L is shown in Scheme 1. The nucleophilic substitution of the chloride **2**[13,14] with dimethyl iminodiacetate (a) results in the intermediate **3**, and its consequent basic hydrolysis and purification with basic DOWEX eluted in acetic acid (b) results in the ligand H_3L, in good yields.

(19) Herrador, M. A.; González, A. G. *Talanta* **2002**, *56*, 769–775.
(20) Martell, A.; Motekaitis, R. J. *Determination and Use of Stability Constants*, 2nd ed.; VCH: New York, 1992.
(21) Ausubel, F. M.; Brent, R.; Kingston, R. E.; Moore, D. D.; Seidman, J. G.; Smith, J. A.; Struhl, K. In *Short Protocols in Molecular Biology: A Compendium of Methods from Current Protocols in Molecular Biology*; Wiley: New York, 1999.
(22) *HiSpeed Plasmid Purification Handbook*; Qiagen: Hilden, Germany, 2001; p 46.
(23) Jin, Y.; Cowan, J. A. *J. Am. Chem. Soc.* **2005**, *127*, 8408–8415.
(24) Sreedhara, A.; Freed, J. D.; Cowan, J. A. *J. Am. Chem. Soc.* **2000**, *122*, 8814–8824.

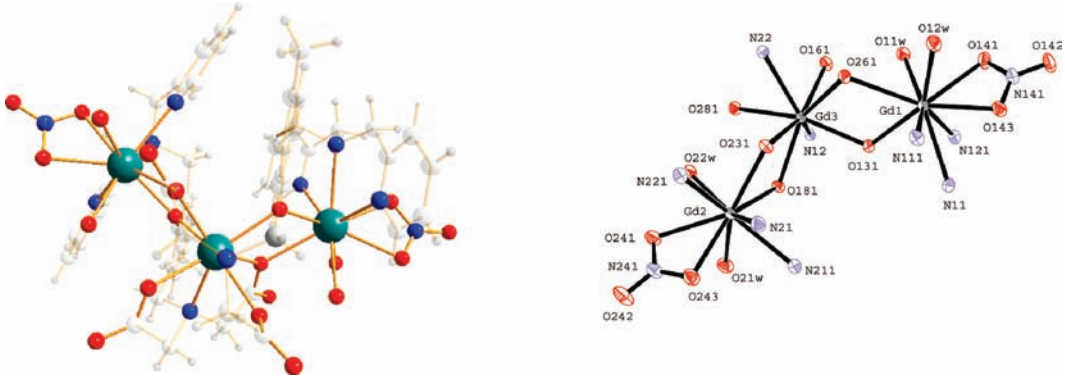

Figure 1. Molecular structure of the cation $[Gd_3(C_{50}H_{58}N_{10}O_{20})]^+$ (right) and ORTEP plot of the coordination environment around the metal centers in complex **1** (left, other atoms are omitted for clarity). Ellipsoid at the 40% probability level.

Scheme 1. Synthetic Route Used for the Preparation of the Unsymmetrical Ligand H_3L

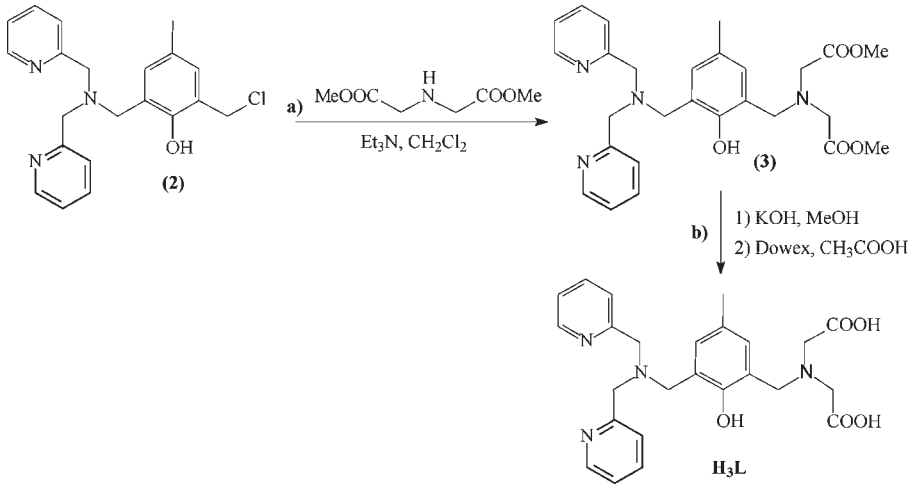

Two H_3L ligands are able to coordinate three Gd^{III} ions held together by phenolate and carboxylate pendant arms forming bridges. Infrared spectroscopy was essential for the preliminary characterization of the ligand and the complex. The $[Gd_3L_2(NO_3)_2(H_2O)_4]NO_3 \cdot 8H_2O$ complex (**1**) shows stretching frequencies typical of bidentate nitrates (1482 and 1295 cm^{-1}) and stretching bands of free (non-coordinated) anionic nitrate (1386 cm^{-1}), which were assigned by the difference between the spectra of complex **1** and H_3L.

X-ray Structure Characterization. Complex **1** crystallizes in an orthorhombic cell, space group *Pcab*. An Oak Ridge thermal-ellipsoid plot (ORTEP)[25] view of the cation complex is presented in Figure 1. The crystallographic data and the main bond distances/angles are given in Tables 1 and 2, respectively. The resolution of the crystal structure of **1** shows an asymmetric unit composed of a cation complex $[Gd_3L_2(NO_3)_2(H_2O)_4]^+$ and a nitrate anion as the counterion with eight water molecules as the crystallization solvent.

Figure 1 shows the structure of the monocationic trinuclear complex which is composed of three Gd^{III} ions, two L^{3-} ligands (with phenolate and carboxylate pendant arms forming bridges), four coordinated water molecules and two coordinated bidentate nitrates. The two terminal metal ions, Gd1 and Gd2, show the same coordination environment, where each ion is nona-coordinated to one tertiary amine nitrogen atom N11 (or N21), two pyridine nitrogen atoms N121 and N111 (or N211 and N221), one phenolate oxygen atom O131 (or O261), and one carboxylate oxygen atom O231 (or O181), in addition to the two oxygen atoms of the bidentate nitrate O141 and O143 (or O241 and O243) and two water molecules coordinated to a terminal metal. The central metal, Gd3, is octacoordinated to two tertiary amine nitrogen atoms N12 and N22, two phenolate oxygen atoms O231 and O131, and four carboxylate oxygen atoms O281, O261, O181, and O161.

Since the two terminal metal ions, Gd1 and Gd2, show the same coordination environment, we can observe similar lengths and bond angles. For example, the bond distance Gd1−N11 (tertiary amine) is 2.653 Å, which is similar to that of Gd2−N21 (2.651 Å) and the angle N121−Gd1−N111 is 129.30°, slightly greater than the corresponding angle N221−Gd2−N211 (128.21°).

The central metal Gd3 is coordinated to the four carboxylate groups from the two ligands L^{3-}, and it is possible to observe the differences between the average bond lengths: 2.419 Å for Gd3−O(monodentate carboxylate) and 2.408 Å for Gd3−O(carboxylate bridge).

The separations Gd1···Gd3 and Gd3···Gd2 (4.0482 Å and 4.0643 Å, respectively) are similar to the Gd···Gd separations found in the homotrinuclear complexes with amine phenolate, multidentate ligands.[26]

(25) Spek, A. L. *J. Appl. Crystallogr.* **2003**, *36*, 7–13.

(26) Setyawati, I. A.; Liu, S.; Rettig, S. J.; Orvig, C. *Inorg. Chem.* **2000**, *39*, 496–507.

Table 2. Selected Bond Lengths [Å] and Angles [deg] for Complex **1**

Gd1−O131	2.389(3)	Gd2−O21W	2.416(4)
Gd1−O12W	2.404(4)	Gd2−O243	2.444(4)
Gd1−O11W	2.446(4)	Gd2−O241	2.550(4)
Gd1−O143	2.489(4)	Gd2−N221	2.551(5)
Gd1−O141	2.529(4)	Gd2−N211	2.594(5)
Gd1−N121	2.539(5)	Gd2−N21	2.655(4)
Gd1−N111	2.608(5)	Gd2−O181	2.670(3)
Gd1−O261	2.645(3)	Gd2−Gd3	4.0481(4)
Gd1−N11	2.653(5)	Gd3−O231	2.377(3)
Gd1−Gd3	4.0643(4)	Gd3−O131	2.380(3)
Gd2−O231	2.401(3)	Gd3−O281	2.406(4)
Gd2−O22W	2.404(4)	Gd3−O161	2.409(3)
Gd3−O261	2.417(3)	Gd3−N12	2.536(4)
Gd3−O181	2.422(3)	Gd3−N22	2.541(4)
O131−Gd1−O12W	140.92(13)	O131−Gd1−O12W	140.92(13)
O131−Gd1−O11W	85.52(13)	O131−Gd1−O11W	85.52(13)
O12W−Gd1−O11W	82.33(14)	O12W−Gd1−O11W	82.33(14)
O131−Gd1−O143	143.11(13)	O131−Gd1−O143	143.11(13)
O12W−Gd1−O143	74.53(14)	O12W−Gd1−O143	74.53(14)
O11W−Gd1−O143	115.88(14)	O11W−Gd1−O143	115.88(14)
O131−Gd1−O141	135.81(13)	O131−Gd1−O141	135.81(13)
O12W−Gd1−O141	70.07(14)	O12W−Gd1−O141	70.07(14)
O11W−Gd1−O141	65.51(13)	O11W−Gd1−O141	65.51(13)
O143−Gd1−O141	50.45(13)	O143−Gd1−O141	50.45(13)
O131−Gd1−N121	75.68(13)	O131−Gd1−N121	75.68(13)
O12W−Gd1−N121	139.08(15)	O12W−Gd1−N121	139.08(15)
O11W−Gd1−N121	84.34(14)	O11W−Gd1−N121	84.34(14)
O143−Gd1−N121	77.00(15)	O143−Gd1−N121	77.00(15)
O141−Gd1−N121	69.18(14)	O141−Gd1−N121	69.18(14)
O131−Gd1−N111	98.95(13)	O131−Gd1−N111	98.95(13)
O12W−Gd1−N111	73.89(15)	O12W−Gd1−N111	73.89(15)
O11W−Gd1−N111	147.36(15)	O11W−Gd1−N111	147.36(15)
O143−Gd1−N111	79.20(15)	O143−Gd1−N111	79.20(15)
O141−Gd1−N111	123.66(14)	O141−Gd1−N111	123.66(14)
N121−Gd1−N111	128.19(16)	N121−Gd1−N111	128.19(16)
O131−Gd1−O261	65.62(11)	O131−Gd1−O261	65.62(11)
O12W−Gd1−O261	75.31(12)	O12W−Gd1−O261	75.31(12)
O21W−Gd2−O241	69.60(14)	O21W−Gd2−O241	69.60(14)
O243−Gd2−O241	51.19(12)	O243−Gd2−O241	51.19(12)
O231−Gd2−N221	75.15(13)	O231−Gd2−N221	75.15(13)
O22W−Gd2−N221	81.39(14)	O22W−Gd2−N221	81.39(14)
O21W−Gd2−N221	140.00(14)	O21W−Gd2−N221	140.00(14)
O243−Gd2−N221	79.03(14)	O243−Gd2−N221	79.03(14)
O241−Gd2−N221	70.41(14)	O241−Gd2−N221	70.41(14)
O231−Gd2−N211	96.67(13)	O231−Gd2−N211	96.67(13)
O22W−Gd2−N211	148.76(14)	O22W−Gd2−N211	148.76(14)
O21W−Gd2−N211	74.50(15)	O21W−Gd2−N211	74.50(15)
O243−Gd2−N211	78.62(14)	O243−Gd2−N211	78.62(14)
O241−Gd2−N211	123.50(14)	O241−Gd2−N211	123.50(14)
N221−Gd2−N211	129.33(15)	N221−Gd2−N211	129.33(15)
O231−Gd2−N21	75.74(13)	O231−Gd2−N21	75.74(13)
O22W−Gd2−N21	145.46(14)	O22W−Gd2−N21	145.46(14)
O21W−Gd2−N21	128.28(14)	O21W−Gd2−N21	128.28(14)
O243−Gd2−N21	68.33(13)	O243−Gd2−N21	68.33(13)
O241−Gd2−N21	109.88(13)	O241−Gd2−N21	109.88(13)
N221−Gd2−N21	66.14(14)	N221−Gd2−N21	66.14(14)
N211−Gd2−N21	63.41(15)	N211−Gd2−N21	63.41(15)
O231−Gd2−O181	66.43(11)	O231−Gd2−O181	66.43(11)
O22W−Gd2−O181	69.99(12)	O22W−Gd2−O181	69.99(12)
O21W−Gd2−O181	74.07(12)	O21W−Gd2−O181	74.07(12)
O243−Gd2−O181	147.22(12)	O243−Gd2−O181	147.22(12)
O131−Gd3−N22	138.07(12)	O261−Gd3−N22	69.31(12)
O281−Gd3−N22	65.58(13)	O181−Gd3−N22	131.84(12)
O161−Gd3−N22	75.45(13)	N12−Gd3−N22	123.08(13)

Potentiometric Equilibrium Studies. To determine the possible species present in solution, potentiometric titration experiments of complex **1** were carried out and equilibria involving protonations of the complex and dissociation of coordinated water molecules were proposed (Supporting Information, Figure S1). The results obtained for **1** show the neutralization of 6 mol KOH per mol of complex in the pH range 3.50−11.00. Thus, the equilibrium constants were determined (Table 3) using the BEST7 program,[20] and the values obtained were used to calculate the species distribution curves (Figure 2) and, consequently, the species involved in catalysis.

Table 3. Logarithm K Values for Protonations of the Complex and Dissociation of Coordinated Water Molecules, I = 0.1 mol L^{-1} (KCl)

equilibria	log K
$[Gd_3HL_2^{4+}]/[Gd_3L_2^{3+}]\,[H^+]$	4.78
$[Gd_3H_2L_2^{5+}]/[Gd_3HL_2^{4+}]\,[H^+]$	4.09
$[Gd_3(OH)L_2^{2+}]\,[H^+]/[Gd_3L_2^{3+}]$	−5.61
$[Gd_3(OH)_2L_2^{+}]\,[H^+]/[Gd_3(OH)L_2^{2+}]$	−7.21
$[Gd_3(OH)_3L_2]\,[H^+]/[Gd_3(OH)_2L_2^{+}]$	−9.31
$[Gd_3(OH)_4L_2^{-}]\,[H^+]/[Gd_3(OH)_3L_2]$	−9.36

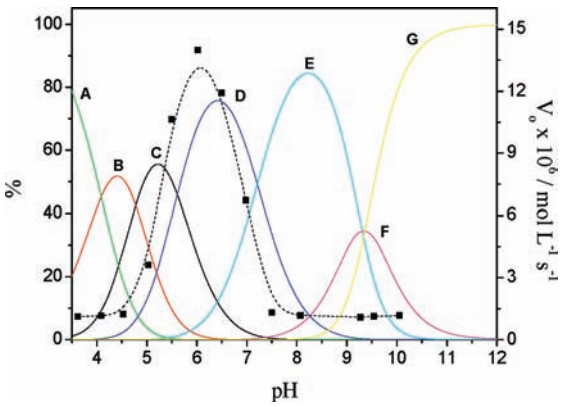

Figure 2. Solid lines represent the species distribution curves of the $Gd_3L_2^{3+}$ system for the dissolution of 0.015 mmol of complex **1** in acetonitrile/water solution, μ = 0.1 mol L^{-1} (KCl) at 25 °C. The dashed line corresponds to the variation in the observed initial rates for the hydrolysis of BDNPP as a function of pH in acetonitrile/water solution. Conditions: [**1**] = 4.0×10^{-5} mol L^{-1}; [BDNPP] = 2×10^{-3} mol L^{-1}; at 25 °C. (A) $[Gd_3H_2L_2]^{5+}$; (B) $[Gd_3HL_2]^{4+}$; (C) $[Gd_3L_2]^{3+}$; (D) $[Gd_3(OH)L_2]^{2+}$; (E) $[Gd_3(OH)_2L_2]^{+}$; (F) $[Gd_3(OH)_3L_2]$; (G) $[Gd_3(OH)_4L_2]^{-}$.

Through the potentiometric results, it is possible to observe protonations of the complex at low pH values, forming protonated $[Gd_3HL_2]^{4+}$ and $[Gd_3H_2L_2]^{5+}$ species. At pH > 5 dissociation of coordinated water molecules is observed, forming the corresponding hydroxide species $[Gd_3(OH)L_2]^{2+}$, $[Gd_3(OH)_2L_2]^{+}$, $[Gd_3(OH)_3L_2]$, and $[Gd_3(OH)_4L_2]^{-}$.

Reactivity Studies. The catalytic activity of complex **1** in the hydrolysis of the activated aryl diester phosphate BDNPP was investigated under conditions of excess substrate, at 25 °C, by following spectrophotometrically the absorbance increase at 400 nm until the conversion of around 1 equiv of the liberated 2,4-dinitrophenolate anion (DNP), using the stopped-flow technique.

The pH dependence of the catalytic activity for BDNPP hydrolysis was investigated in the pH range 3.50−11.00, activity being observed across the whole pH range studied, and a bell-shaped profile was observed with a maximum efficiency at around pH 6. The pH:V_0 profile for complex **1** could be better analyzed when associated with the distribution curves of the species formed in solution (Figure 2), in which the species involved in the catalysis are proposed.

The results in Figure 2 show that at low pH values protonated $[Gd_3H_2L_2]^{5+}$ (A) and $[Gd_3HL_2]^{4+}$ (B) species are formed, with no dissociated water molecule and, consequently, no nucleophile to attack the diester bond, which may explain their low catalytic activities. In the pH

range of around 5.0 to 7.5, higher activity toward BDNPP hydrolysis is observed, where the following equilibria and constants were determined.

$$[Gd_3(L)_2]^{3+} \rightleftharpoons [Gd_3(OH)(L)_2]^{2+} + H^+ \qquad pK_1 = 5.61$$

$$[Gd_3(OH)(L)_2]^{2+} \rightleftharpoons [Gd_3(OH)_2(L)_2]^{+} + H^+ \qquad pK_2 = 7.21$$

These pK_a values are in reasonable agreement with those obtained from the sigmoidal fit of the curve of pH versus V_0 (superimposed curve in Figure 2). These results suggest that the deprotonation of one coordinated water molecule to a metal center in the $[Gd_3L_2]^{3+}$ (C) compound produces the most prominent catalyst in the hydrolysis of BDNPP, the $[Gd_3(OH)L_2]^{2+}$ (D) species. Finally, the decrease in reactivity at pH > 6.5 most probably arises because of the disappearance of the most active species (D), and the formation of the hydroxide species $[Gd_3(OH)_2L_2]^{+}$ (E), $[Gd_3(OH)_3L_2]$ (F), and $[Gd_3(OH)_4L_2]^{-}$ (G). The increase in the negative charges around these species (E−G) may inhibit the nucleophilic attack on the BDNPP substrate (negatively charged) or even lower the binding affinity of the complexes to the substrate, resulting in their low catalytic activity.

Thus, complete kinetic studies were performed at the optimum pH value of 6.0 at which it is believed that the trinuclear $[Gd_3(OH)L_2]^{2+}$ (D) species is the principal species present in solution. The determination of the initial rates as a function of the concentration of the substrate reveals saturation kinetics with Michaelis−Menten-like behavior[27] (Supporting Information, Figure S2). The non-linear least-squares fit of V_0 versus [BDNPP] gives the following values: $K_m = 4.09$ mM, $V_{max} = 2.68 \times 10^{-2}$ mM s^{-1}, and the catalytic constant $k_{cat} = V_{max}/[\mathbf{1}] = 0.67$ s^{-1}. Under these conditions, complex **1** shows a 5 million-fold acceleration in the hydrolysis rate of BDNPP in comparison to the spontaneous hydrolysis.[12] In addition, the catalytic activity of **1** in the hydrolysis is around 4×10^3 times faster than the reaction catalyzed by $Gd(NO_3)_3 \cdot 6H_2O$, under the same experimental conditions (Supporting Information, Table T1).

In a recent publication,[28] we reported a dinuclear gadolinium species (in solution) with a high efficiency in the hydrolysis of BDNPP, which is around 25 times faster than that of complex **1**, indicating that the trinuclear gadolinium complex probably displays a different action mechanism toward BDNPP hydrolysis compared to the dinuclear species. However, further studies are necessary to identify the mechanism involved when complex **1** is the catalyst. On the other hand, complex **1** has a catalytic constant around 20 times higher than the value observed for the hydrolysis reaction of the same substrate using different Ln^{III} complexes with bis-tris propane (BTP) as the catalyst.[29]

To assess the possible hydrolysis of the monoester 2,4-dinitrophenylphosphate (DNPP), one of the products formed from the hydrolysis reaction of the diester BDNPP, the stoichiometric reaction between complex **1** and the BDNPP substrate was monitored. It was observed that 2 equiv of DNP are released in 2 h, at 25 °C, which indicates the hydrolysis of both the mono- and the diester.

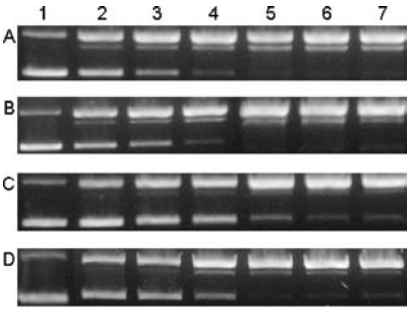

Figure 3. Plasmid DNA cleavage promoted by complex **1** at pH 6.5, 7.0, 7.5, and 8.0 (A, B, C, and D, respectively), at 50 °C and incubation for 7 h. Lane 1: pBSK II DNA (40 μM bp). Lanes 2−7: DNA + complex 1 10, 20, 30, 60, 90, and 125 μM, respectively. Reactions were performed in 25 mM PIPES buffer (pH 6.5, 7.0 and 7.5) or HEPES buffer pH 8.0 in CH_3CN:H_2O 25:75%.

As our main goal was to obtain an effective catalyst, a hydrolysis reaction of BDNPP (2×10^{-3} M) promoted by complex **1** (4×10^{-5} M) at 445 nm, pH 6, and 25 °C was also monitored. These data revealed that the complex is able to hydrolyze 6 molecules of substrate in 1 h and can be considered as an efficient catalyst.

DNA Interaction. The influence of complex concentration and pH on the nucleic acid cleavage activity were investigated at pH 6.5, 7.0, 7.5, and 8.0 with selected complex **1** concentrations (0−125 μM), at 50 °C (Figure 3). These results show that complex **1** effectively promotes the cleavage of supercoiled (form I) DNA to nicked circular (form II) and linear (form III) DNA with higher activity at pH 7, a value which is one pH unit higher than that found in the hydrolysis of the BDNPP substrate. However, the species suggested as the most catalytic $[Gd_3(OH)L_2]^{2+}$ (D) is still the principal species present in solution at around this pH range (Figure 2).

Thus, kinetic studies were performed at pH 7, under conditions of excess complex over substrate (DNA), at 50 °C (Supporting Information, Figure S3), and the following kinetic parameters were obtained: $k'_{cat} = 3.42$ h^{-1}, $K_m = 4.57 \times 10^{-4}$ M and $k'_{cat}/K_m = 7.48 \times 10^3$ M^{-1} h^{-1}, providing a 100 million-fold rate enhancement over the uncatalyzed DNA cleavage.[30] Furthermore, complex **1** shows a higher catalytic constant in comparison to the value of $k_{cat} = 0.47$ h^{-1} observed for the binuclear gadolinium species previously reported by us,[28] indicating different mechanisms of action for the complexes with regard to DNA cleavage.

To investigate the mechanism of action of complex **1** toward DNA cleavage, experiments were performed in the presence of dimethyl sulfoxide, a hydroxyl radical scavenger. The cleavage activity of **1** was not affected by the presence of DMSO (Supporting Information, Figure S4), suggesting that diffusible HO$^{\bullet}$ radicals are not involved in the cleavage of plasmid DNA. These results are in agreement with the known hydrolytic action of lanthanide ions toward the cleavage of phosphate esters.[31,32]

(27) Stryer, L. *Bioquímica*. 4nd ed.; Guanabara Koogan; Rio de Janeiro, Brazil, 1996; pp 180−185.
(28) Camargo, M. A.; Neves, A.; Bortoluzzi, A. J.; Szpoganicz, B.; Martendal, A.; Murgu, M.; Fischer, F. L.; Terenzi, H.; Severino, P. C. *Inorg. Chem.* **2008**, *47*, 2919–2921.
(29) Longhinotti, E.; Domingos, J. B.; da Silva, P. L. F.; Szpoganicz, B.; Nome, F. *J. Phys. Org. Chem.* **2005**, *18*, 167–172.
(30) Radzicka, A.; Wolfenden, R. *Science* **1995**, *267*, 90–93.
(31) Kulkarni, A.; Patil, S. A.; Badami, P. S. *Eur. J. Med. Chem.* **2009**, *44*, 2904–2912.
(32) Baykal, U.; Akkaya, E. U. *Tetrahedron Lett.* **1998**, *39*, 5861–5864.

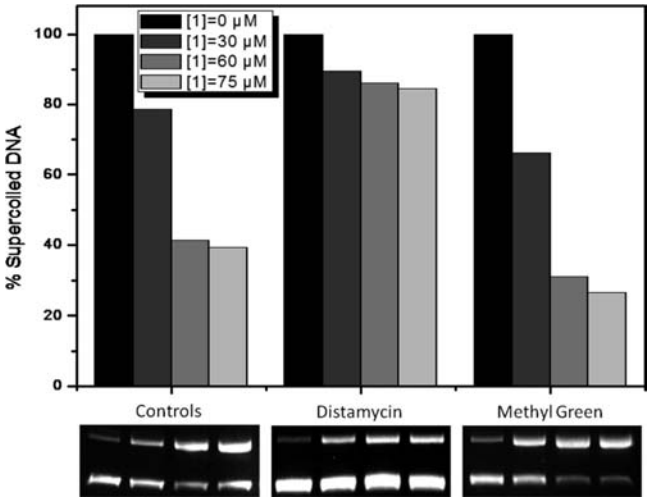

Figure 4. Analysis of plasmid DNA cleavage (pBSK-II, 40 μM bp) catalyzed by complex **1**, in the absence and presence of distamycin and methyl green (50 μM), after incubation for 6 h at 50 °C, at pH 7.0 (PIPES buffer 25 mM).

To obtain a greater understanding of the specific contact surfaces between the catalytic species and the DNA helix, studies were carried out with distamycin, a specific minor groove binder and methyl green, a major groove binder. The catalytic activity of complex **1** appears not to be partially influenced by the presence of distamycin (Figure 4), and not at all by methyl green, suggesting its specificity for the minor groove of DNA.

Conclusions

In summary, we have synthesized and characterized the new trinuclear gadolinium complex $[Gd_3L_2(NO_3)_2(H_2O)_4]NO_3 \cdot 8H_2O$ (**1**) with the new unsymmetrical ligand H_3L. Complex **1** shows efficient hydrolase-like activity toward the BDNPP substrate and DNA, with regio-specificity in the DNA binding, indicating its potential action as a chemical nuclease. Finally, the synthetic routes described for the preparation of the ligand H_3L and the trinuclear Gd complex can be used as general methods for the preparation of trinuclear lanthanide complexes with H_3L. The synthesis of the corresponding trinuclear Tb^{III} and Eu^{III} complexes, along with kinetic and luminescent studies, is in progress to help elucidate the mechanism involved in the catalytic cycle and unambiguously identify the active species. Furthermore, attempts to synthesize heterotrinuclear lanthanide complexes will also be the subject of future research to exploit their unique luminescent properties.

Acknowledgment. Financial support was received from CNPq, INCT-catálise, INCT-Biologia Estrutural e Bioimagem, FAPESC, and M.A.C. is grateful to CNPq for a postdoc grant (PNPD-151665/2008-7). Prof. Dr. Antônio C. Joussef and Sandro L. Mireski kindly helped with the organic purification methods and Prof. Dr. Marcos N. Eberlin and Vanessa G. Santos with the ESI analyses.

Supporting Information Available: X-ray crystallographic file in CIF format; Figures S1−S4 and Table T1 in PDF format. This material is available free of charge via the Internet at http://pubs.acs.org. Full tables of crystallographic data of complex **1** (except structure factors) were deposited at Cambridge Structural Database (CCDC 752704), and these data are available free of charge from: CCDC, 12 Union Road, Cambridge, CB2 1EZ, UK (Fax: +44−1223−336−003; e-mail: deposit@ccdc.cam.ac.uk or http://www.ccdc.cam.ac.uk.